Research Article

Shuguang Li, Waseh Farooq, Aamar Abbasi, Sami Ullah Khan, Maimona Rafiq*, Muhammad Ijaz Khan, Barno Sayfutdinovna Abdullaeva, Fuad A. Awwad, and Emad A. A. Ismail

Coupled heat and mass transfer mathematical study for lubricated non-Newtonian nanomaterial conveying oblique stagnation point flow: A comparison of viscous and viscoelastic nanofluid model

https://doi.org/10.1515/phys-2023-0141
received May 11, 2023; accepted October 30, 2023

Abstract: The lubrication phenomenon plays a novel role in the chemical industries, manufacturing processes, extrusion systems, thermal engineering, petroleum industries, soil sciences, *etc*. Owing to such motivated applications, the aim of the current work is to predict the assessment of heat and mass transfer analysis for non-Newtonian nanomaterial impinging over a lubricated surface. The flow is subject to the oblique stagnation point framework. The lubricated phenomenon is observed due to viscoelastic nanofluid. The impacts of chemical reaction are also endorsed. The fundamental conservation laws are utilized to model the flow problem and similarity transformation are used to transform the governing system of partial differential equations into ordinary differential equations. A thin layer of power law lubricant is used to enhance the lubrication features. The numerical object assessment regarding the simulation process is captured by implementing the Keller Box scheme. The physical characterization endorsing the thermal fluctuation with flow parameters is inspected.

Keywords: viscoelastic fluid, chemical reaction, lubricated surface, heat and mass transfer, numerical solution

*** Corresponding author: Maimona Rafiq,** Department of Mathematics, COMSATS University Islamabad, Attock 43600, Pakistan, e-mail: maimona_88@hotmail.com
Shuguang Li: School of Computer Science and Technology, Shandong Technology and Business University, Yantai, 264005, China
Waseh Farooq, Aamar Abbasi: Department of Mathematics, University of Azad Jammu and Kashmir, Muzaffarabad, 13100, Pakistan
Sami Ullah Khan: Department of Mathematics, Namal University, Mianwali 42250, Pakistan
Muhammad Ijaz Khan: Department of Mechanical Engineering, Lebanese American University, Beirut, Lebanon; Department of Mathematics and Statistics, Riphah International University, I-14, Islamabad 44000, Pakistan
Barno Sayfutdinovna Abdullaeva: Vice-Rector for Scientific Affairs, Tashkent State Pedagogical University, Tashkent, Uzbekistan
Fuad A. Awwad, Emad A. A. Ismail: Department of Quantitative Analysis, College of Business Administration, King Saud University, P.O. Box 71115, Riyadh 11587, Saudi Arabia

Nomenclature

(a', b')	dimensionless constants
(C_1, C_2)	constant of integration
C_{f}	dimensionless skin friction coefficient
C_{w}	surface concentration
C_{∞}	free surface concentration
D_{B}	Brownian diffusion coefficient
D_{T}	thermophoresis diffusion coefficient
j_{w}	mass flux
k	thermal conductivity
k_0	second grade fluid parameter
k^*	mean absorption constant
k_1	dynamic coefficient of viscosity
Le	Lewis number
$\mathrm{N_b}$	Brownian motion parameter
Nt	thermophoresis parameter
Nu_x	Nusselt number
p	pressure
Pr	Prandtl number
Q	flow rate
q_{w}	radiative heat flux
Re	Reynolds number
R_{d}	radiation parameter
Sh	Sherwood number

T_w	surface temperature
(u,v)	components of velocity
(U,V)	axial and tangential velocities of lubricant
$\boldsymbol{u_e}$	axial velocity component at free stream
v_e	tangential velocity component at free stream
T_w	surface temperature
T_∞	free surface temperature
$\delta(x)$	lubricated surface width
ρ	density
μ	dynamic viscosity
α	thermal diffusivity
τ	effective heating nanoparticles capacitance to nanofluid heat capacity
σ^*	Stefan–Boltzmann constant
α_1	viscoelastic parameter
β_c	chemical reaction parameter
λ	slip parameter
γ	shear at the free stream
τ_w	wall shear stress component

1 Introduction

In fluid mechanics, stagnation point flow is defined as the movement of fluid near the solid surface. Fluid splits up into two surfaces or deviates its route when it approaches the surface. Physical importance of stagnation point flows is noteworthy since they utilize to commute velocity gradients as well as estimate mass or heat transfer and skin friction in the stagnation zone. A comprehensive literature survey regarding stagnation points flow owing to its eminent applications has been presented by numerous investigators. Hiemenz [1] scrutinized the two dimensional motion of viscous fluid in the zone of stagnation point on a flat plate. Homann [2] discussed the axisymmetric flow in the zone of stagnation point on flat surface. Hannah [3] analyzed the Homan flow of stagnation point over disk which was the broadening work of Homan's genuine inquiry involving the plate flow following the stagnation phenomenon. The moving surface according to the stagnation point situation, a two-dimensional, viscous and incompressible flow was examined by Rott [4]. On a flat plate, Weidman and Mahalingam [5] did their research relating to the axisymmetric flow of stagnation point problem. Mahapatra and Gupta [6] examined stagnation point flow approaching the stretched surface. The flow analysis for a viscous fluid impinging obliquely on stretched sheet was carried out by Lok *et al.* [7]. Nadeem *et al.* [8] investigated the dilemma of stagnation point's flow for the Jeffrey fluid on shrinking sheet. Weidman and Sprague [9] investigated flow caused by a plate moving in a normal to stagnation point flow. Irrotational stagnation point flows by Hiemenz and Homan were contemplated. Two Hiemenz planar stagnation point flows that were normal to a uniform plate were explored by Weidman [10] for their interaction.

The approaching impinging flow on a surface creates a point of stagnation where the fluid velocity drops to zero. The fluid flow surrounding this stagnation point is known as stagnation point flow. In fact, stagnation point phenomenon preserved the extension of Hiemenz phenomenon. Hiemenz flow, also known as the oblique stagnation point flow, involves the flow of a liquid that adjusts to the surface at a right angle. The prime investigation on this subject was carried out by Stuart [11]. Tamada [12] studied the stagnation point flow impinging obliquely over a oscillating flat surface. The outcomes for two-dimensional oblique stagnation point flow are presented through calculating exact solutions by Dorrepaal [13]. Reza and Gupta [14] analyzed the non-orthogonal situation for the stagnation point where pressure gradient plays an important role. Weidman and Putkaradze [15] investigated the stagnation point impact for circular cylinder without considering the role of displacement thickness and pressure variation. The micropolar material flow with oblique stagnation point observations was determined by Lok *et al.* [16].

Heat is an energy form which distributes energy to the substance's molecules in an accelerative way, and gathers this kinetic energy on a massive level. Consequently, as this energy approaches its maximum or minimum point, the molecules or atoms are liberated from interatomic forces of attraction and alter their state. Heat transfer is a mechanism that happens when the temperatures of two substances change *i.e.,* from warm to cold or from cold to warm substance. Heat transport and flow using the second grade fluid across a stretched sheet were studied by researchers Dandapat and Gupta [17]. The transmission of heat in a flow of stagnation point across a stretched sheet was studied by Mahapatra and Gupta [18]. Analysis of analytical solutions for the exchange of thermal energy and axisymmetric flow in a viscoelastic fluid across a stretched sheet was done Hayat and Sajid [19]. Attia [20] determined the progress of heat transfer near the stagnation point region in a porous medium for second grade fluid. In a boundary layer stagnation point flow toward an extending or contracting sheet, melting heat transfer was examined by Bachok *et al.* [21]. The heating determination deduced for Jeffrey fluid *via* flat surface with non-orthogonal stagnation framework was examined by Arshad *et al.* [22]. In another attempt, Bano *et al.* [23] described a mathematical model to discuss the heat transfer characteristics

over a stretching cylinder. Labropulu *et al.* [24] reported the effects of elasticity involving the heat transfer pattern. Abbasi *et al.* [25] studied about radiated phenomenon for obliquely moving surface.

The nanofluids attract the researchers due to many applications in industry and biomedical science like cancer therapy, cooling and heating processes, *etc*. Many organic and inorganic fluids like grease, oil and ethyl glycol have poor thermal and electric conductivity. Many techniques are proposed in the literature to enhance the thermal and electric properties of these working fluids. By adding nanoparticles up to size 1–100 nm having large thermal and electric conductivity in the base fluid is commonly used by many researchers and scientists. These fluids were characterized as nanofluids for the first time by Choi and Eastman [26]. Later on, Das *et al.* [27] carried out a study to prove that by addition of 1% of nanoparticles in a base fluid can enhance its thermal properties up to 100% more than the base fluid. Buongiorno [28] deduced the nanofluid transport applications *via* theoretical study. Later on, many theoretical studies used the Buongiorno model to investigate the stagnation point flows of nanofluids. Hamid *et al.* [29] identified the pattern of stagnation point for nanoparticles flow *via* stretched surface. Roşca *et al.* [30] investigated the response of the same phenomenon for boundary effected flow with flat surface due to nanofluid. Abbasi *et al.* [31] studied about slip impact with circular moving cylinder. Abbasi *et al.* [32] reported the stagnation outcomes of Maxwell nanomaterial over a stretching cylinder with different heat transfer features. Mahmood *et al.* [33] examined the effects of lubrication while elaborating the oblique stagnation onset of flat surface conveying the viscous fluid flow. It is noted that the temperature of nanofluid is large over lubricated surface as compared to rough surface. Abbasi *et al.* [34] imposed the microorganisms suspension for nanofluid *via* obliquely lubricated space. The representation of dual solution for lubricated nanofluid *via* oscillating surface was reported by Nadeem and Khan [35]. Bao *et al.* [36] predicted the hybrid nanofluid heat transfer performances for solar collectors. Selim *et al.* [37] disclosed the magnetic force association for fluctuating the thermal prospective of nanomaterials. Hanafi *et al.* [38] pronounced the mathematical model for expressing the nanofluid with suspension of aluminum and copper nanoparticles. Ghafouri and Toghraie [39] performed the experimental analysis for nanofluid in view of variable thermal conductivity. Sundar [40] presented a comprehensive review of hybrid nanofluid with heat exchanger applications. The physical significance of micro-channels are depicted in previous literature [41–43] and the impact of hydro-dynamics in flow with different geometries are reported in previous research works [44–46].

After presenting an inspired analysis on current topic, it is mentioned that different research studies on nanofluids are presented in various flow configurations. However, the thermal applications of nanofluids due to obliquely lubricated surface have not been focused yet. The applications of nanoparticles are interesting in lubricated phenomenon. With these motivations in mind, the aim of the current work is to analyze the two-dimensional stagnation point flow of second grade fluid on a flat rigid obliquely lubricated surface. This phenomenon is commonly observed when a jet of fluids strikes obliquely on a lubricated surface. The main aim of our study is to examine the oblique stagnation point flow of second grade nanofluid over a lubricated surface in the presence of linear thermal radiation. The reactive species with first order relations have been utilized to analyze the phenomenon. The motivations behind choice of second grade fluid is satisfied with novel rheology and interesting dynamics. The problem is illustrated and modeled with partial differential system. The implicit finite difference scheme along with quasi linearization is used to simulate the different flow and heat transfer features. The physical impact of problem with variation in parameters is observed.

2 Problem formulation

The current mathematical model is used to simulate 2D stagnation point assessment of viscoelastic fluid characterized by second grade fluid over a flat lubricated surface. For mathematical formulation, Cartesian coordinate system is used such that the fluid flowing along the x-axis and y-axis is perpendicular to the lubricated surface with variable width $\delta(x)$. Furthermore, the temperature T_w and concentration of the nanoparticles C_w are same at the surface of the sheet and at $y = 0$. The free surface thermal and concentration constraints are identified by T_∞ and C_∞, respectively. The axial and tangential velocity components at free stream are u_e and v_e (Figure 1).

The investigation of nanofluid in the present problem is predicated by using Buongiorno two phase fluid model along with Rosseland approximation for linear thermal radiation. In order to describe the diffusion rates the chemical reaction of first order is taken in the concentration of nanoparticles.

After using the aforementioned restrictions and conditions, the formulated equations are [33,35] as follows:

$$\frac{\partial u}{\partial x} + \frac{\partial v}{\partial y} = 0, \tag{1}$$

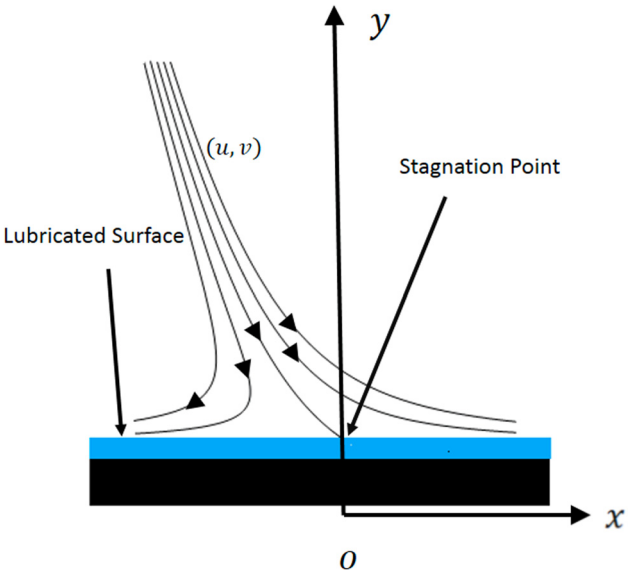

Figure 1: Flow geometry.

$$\frac{\partial u}{\partial x}+\frac{\partial u}{\partial y}=-\frac{1}{\rho}\frac{\partial p}{\partial x}+\frac{\mu}{\rho}\left(\frac{\partial^2 u}{\partial x^2}+\frac{\partial^2 u}{\partial y^2}\right)+\frac{k_0}{\rho}\left[2\frac{\partial}{\partial \bar{x}}\left\{u\frac{\partial^2 u}{\partial x^2}-\frac{\partial u}{\partial y}\left(\frac{\partial u}{\partial y}+\frac{\partial v}{\partial x}\right)+v\frac{\partial^2 u}{\partial x\partial y}-2\left(\frac{\partial u}{\partial x}\right)^2\right\}+\frac{\partial}{\partial y}\left\{v\frac{\partial^2 u}{\partial y^2}+v\frac{\partial^2 v}{\partial x\partial y}+u\frac{\partial^2 u}{\partial x\partial y}+u\frac{\partial^2 v}{\partial x^2}-2\left(\frac{\partial v}{\partial y}\frac{\partial u}{\partial y}+\frac{\partial u}{\partial x}\frac{\partial v}{\partial x}\right)\right\}\right], \tag{2}$$

$$\frac{\partial v}{\partial x}+\frac{\partial v}{\partial y}=-\frac{1}{\rho}\frac{\partial p}{\partial y}+\frac{\mu}{\rho}\left(\frac{\partial^2 v}{\partial x^2}+\frac{\partial^2 v}{\partial y^2}\right)+\frac{k_0}{\rho}\left[\frac{\partial}{\partial x}\left\{u\frac{\partial^2 v}{\partial x^2}+v\frac{\partial^2 u}{\partial y^2}+u\frac{\partial^2 u}{\partial x\partial y}+v\frac{\partial^2 v}{\partial x\partial y}-2\left(\frac{\partial u}{\partial y}\frac{\partial v}{\partial y}+\frac{\partial u}{\partial x}\frac{\partial v}{\partial x}\right)\right\}+2\frac{\partial}{\partial y}\left\{u\frac{\partial^2 v}{\partial x\partial y}-\frac{\partial v}{\partial x}\left(\frac{\partial u}{\partial y}+\frac{\partial v}{\partial x}\right)-2\left(\frac{\partial v}{\partial x}\right)^2+v\frac{\partial^2 v}{\partial y^2}\right\}\right], \tag{3}$$

$$u\frac{\partial T}{\partial x}+v\frac{\partial T}{\partial y}=\alpha\left(\frac{\partial^2 T}{\partial x^2}+\frac{\partial^2 T}{\partial y^2}\right)+\frac{1}{\rho c_p}\left(\frac{16\sigma^* T_\infty^3}{3k^*}\frac{\partial^2 T}{\partial y^2}\right)+\tau\left[D_B\left(\frac{\partial T}{\partial x}\frac{\partial T}{\partial y}+\frac{\partial C}{\partial x}\frac{\partial C}{\partial y}\right)+\frac{D_T}{T_\infty}\left[\left(\frac{\partial T}{\partial x}\right)^2+\left(\frac{\partial T}{\partial y}\right)^2\right]\right], \tag{4}$$

$$u\frac{\partial C}{\partial x}+v\frac{\partial C}{\partial y}=D_B\left(\frac{\partial^2 C}{\partial x^2}+\frac{\partial^2 C}{\partial y^2}\right)+\frac{D_T}{T_\infty}\left(\frac{\partial^2 T}{\partial x^2}+\frac{\partial^2 T}{\partial y^2}\right)-K_1(C-C_\infty), \tag{5}$$

where ρ stands for the density, u and v are the components of velocity, k_0 is the second grade fluid parameter, μ represents the dynamic viscosity, p is the pressure, α is the thermal diffusivity, $\tau=(\rho c)_p/(\rho c)_f$ expressed the effective heating nanoparticles capacitance to nanofluid heat capacity of nanoparticles, D_B is the Brownian diffusion coefficient, D_T is the thermophoresis diffusion coefficient, σ^* is Stefan–Boltzmann constant and k^* is the mean absorption constant.

The no-slip boundary condition at the surface implies

$$U(x,0)=V(x,0)=0, \tag{6}$$

where U and V are the axial and tangential velocities of lubricant.

In order to obtain the boundary condition at the lubricant and non-Newtonian fluid interface, the continuity of shear stresses and velocities is used.

$$\mu\frac{\partial u}{\partial y}+k_0\left(v\frac{\partial^2 u}{\partial y^2}-2\frac{\partial u}{\partial y}\frac{\partial v}{\partial y}+\frac{\partial^2 u}{\partial x\partial y}\right)=\mu_L\frac{\partial U}{\partial y}, \tag{7}$$

in which

$$\mu_L=k_1\left(\frac{\partial U}{\partial y}\right)^{n-1}, \tag{8}$$

where k_1 is the dynamic coefficient of viscosity. For linear lubricated velocity $U(x,y)$, the relation is

$$U(x,y)=\frac{\check{U}(x)y}{\delta(x)}, \tag{9}$$

with lubricant thickness $\delta(x)$.

Now the relation between the thickness of the lubricant and flow rate Q is

$$\delta(x)=\frac{2Q}{\check{U}}. \tag{10}$$

using Eqs. (9) and (10), Eq. (7) takes the form

$$\mu\frac{\partial u}{\partial y}+k_0\left(v\frac{\partial^2 u}{\partial y^2}-2\frac{\partial u}{\partial y}\frac{\partial v}{\partial y}+\frac{\partial^2 u}{\partial x\partial y}\right)=k_1\left(\frac{1}{2Q}\right)^n\check{U}^{2n}. \tag{11}$$

The continuity of horizontal component of velocity components implies

$$u=\check{U}. \tag{12}$$

Substituting Eq. (12) in Eq. (11), the continuity of shear stresses takes the form

$$\frac{\partial u}{\partial y}+\frac{k_0}{\mu}\left(v\frac{\partial^2 u}{\partial y^2}-2\frac{\partial u}{\partial y}\frac{\partial v}{\partial y}+\frac{\partial^2 u}{\partial x\partial y}\right)=\frac{k_1}{\mu}\left(\frac{1}{2Q}\right)^n u^{2n}. \tag{13}$$

If a' and b' are dimensionless constants, the velocities at free stream take the form [1]

$$u_e = ax + b(y - b'), v_e = -a(y - a'). \tag{14}$$

New variables are:

$$u = axF'(\eta) + aG'(\eta), v = -\sqrt{av}F(\eta), x_1 = x\sqrt{\frac{a}{\nu}},$$
$$\eta = y\sqrt{\frac{a}{\nu}}\theta(\eta) = \frac{T - T_\infty}{T_w - T_\infty}, \phi(\eta) = \frac{C - C_\infty}{C_w - C_\infty}.$$

After equating the coefficient of x_1^0 and x_1 and integrating once with respect to y, the modeled equation can be written as follows:

$$F''' - F'^2 + FF'' - \alpha_1(FF^{iv} - 2F'F''' + F''^2) + C_1 = 0, \tag{15}$$

$$G''' - F'G' + FG'' - \alpha_1(FG^{iv} + G''F'' - F'G''' - G'F''') + C_2 = 0, \tag{16}$$

$$\left(1 + \frac{4}{3}R_d\right)\theta'' + \Pr F\theta' + \Pr Nb\theta'\phi' + \Pr Nt\theta'^2 = 0, \tag{17}$$

$$\phi'' + LeF\phi' + \frac{Nt}{Nb}\theta'' - Le\beta_c\phi = 0, \tag{18}$$

where C_1 and C_2 are the constants of integration, $\alpha_1 = k_0 a/\rho\nu$ represents viscoelastic parameter, $\Pr = \nu/\alpha$ is the Prandtl number, $Le = \nu/D_B$ is the Lewis number, $Nt = \frac{\tau D_T(T_w - T_\infty)}{T_\infty \nu}$ is the thermophoresis parameter, $Nb = \frac{\tau D_B(C_w - C_\infty)}{C_\infty \nu}$ is the Brownian motion parameter, $R_d = \frac{4\sigma^* T_\infty^3}{k^*}$ is the radiation parameter and $\beta_c = \frac{K_1(C_w - C_\infty)}{\nu}$ is the chemical reaction parameter.

The associated boundary conditions in dimensionless form are

$$F(0) = 0, F''(0) + 3\alpha_1 F'(0)F''(0) = \lambda(F'(0))^{2n}, \quad F'(\infty) = 1, F''(\infty) = 0, \tag{19}$$

$$G(0) = 0, G''(0) + \alpha_1(G'(0)F''(0) + 2G''(0)F'(0)) = 2n\lambda G'(0)(F'(0))^{2n-1}, \tag{20}$$

$$G''(\infty) = \gamma, g'''(\infty) = 0, \theta(0) = \phi(0) = 1, \quad \theta(\infty) = \phi(\infty) = 0, \tag{21}$$

where $\lambda = k_1\sqrt{\nu}\, a^{2n}x^{2n-1}/\mu a^{\frac{3}{2}}(2Q)^n$ is the slip parameter. Also, $\gamma = b/a$ is the shear at the free stream. After implementing the boundary conditions at infinity, the constants of integration are $C_1 = 1$ and $C_2 = \gamma(\beta - \varepsilon)$, where $\varepsilon = \eta_\infty - f(\infty)$ and β is the free parameter. Now expressing the wall shear force

$$\tau_w = \left(\mu\frac{\partial u}{\partial y} + k_0\left(\nu\frac{\partial^2 u}{\partial y^2} - 2\frac{\partial u}{\partial y}\frac{\partial v}{\partial y} + \frac{\partial^2 u}{\partial x \partial y}\right)\right)_{y=0}$$
$$q_w = -k\left(\frac{\partial T}{\partial y}\right)_{y=0} - \frac{16\sigma^* T_\infty^3}{3k^*}\left(\frac{\partial T}{\partial y}\right)_{y=0}, j_w = -D_B\left(\frac{\partial C}{\partial y}\right)_{y=0}, \tag{22}$$

with dimensionless form

$$\sqrt{\mathrm{Re}_x}\, C_f = \frac{x_1[F''(0)(1 + 3\alpha_1 F'(0))]}{+ [G''(0) + \alpha_1(G'(0)F''(0) + 2F'(0)G''(0))]}, \tag{23}$$

$$\frac{Nu_x}{\sqrt{\mathrm{Re}_x}} = -\left(1 + \frac{3}{4}R_d\right)\theta'(0), \frac{Sh}{\sqrt{\mathrm{Re}_x}} = -\phi'(0). \tag{24}$$

3 Solution methodology

The simulations are predicted with Keller Box method for solving the Eqs. (15)–(18). The Keller Box technique is supported with finite difference scheme attaining the second-order accuracy. The Keller Box scheme is interesting and various multidisciplinary problems are computed *via* this approach. The numerical scheme is implemented in four steps.

Step 1: Reducing the governing Eqs. (15)–(18) subject to associated boundary conditions in Eqs. (20)–(22) in the system of first-order equations. For this, we consider $F' = U_1, U_1' = V_1, V_1' = W, G' = P_1, P_1' = Q_1, Q_1' = S_1, \theta' = Y_1$ and $\phi' = Z_1$, the governing equations takes the form

$$V_1' - U_1^2 + FV_1 - \alpha_1(FW_1' - 2U_1W_1 + V_1^2) + 1 = 0, \tag{25}$$

$$P_1' - U_1P_1 + FQ_1 - \alpha_1(FS_1' + Q_1V_1 - U_1S_1 - P_1W_1) + \gamma(\beta - \varepsilon) = 0, \tag{26}$$

$$\left(1 + \frac{4}{3}R_d\right)Y_1' + \Pr FY_1 + \Pr NbY_1Z_1 + \Pr NtY_1^2 = 0, \tag{27}$$

$$Z_1' + LeFZ_1 + \frac{Nt}{Nb}Y_1' - Le\beta_c\phi = 0, \tag{28}$$

$$F(0) = 0, V_1(0) + 3\alpha_1 U_1(0)V_1(0) = \lambda(U_1(0))^{2n}, \quad U_1(\infty) = 1, V_1(\infty) = 0, \tag{29}$$

$$G(0) = 0, Q_1(0) + \alpha_1(P_1(0)Q_1(0) + 2Q_1(0)U_1(0)) = 2n\lambda P_1(0)(U_1(0))^{2n-1}, \tag{30}$$

$$Q_1(\infty) = \gamma, S_1(\infty) = 0, \theta(0) = \phi(0) = 1, \quad \theta(\infty) = \phi(\infty) = 0. \tag{31}$$

Step 2: Replacing the derivatives by central finite difference approximation and all dependent and independent variables by taking average of them, we get

$$\begin{aligned}
\frac{F_j - F_{j-1}}{h_j} &= (U_1)_{j-\frac{1}{2}},\\
\frac{(U_1)_j - (U_1)_{j-1}}{h_j} &= (V_1)_{j-\frac{1}{2}},\\
\frac{(V_1)_j - (V_1)_{j-1}}{h_j} &= (W_1)_{j-\frac{1}{2}},\\
\frac{G_j - G_{j-1}}{h_j} &= (P_1)_{j-\frac{1}{2}},\\
\frac{(P_1)_j - (P_1)_{j-1}}{h_j} &= (Q_1)_{j-\frac{1}{2}},\\
\frac{(Q_1)_j - (Q_1)_{j-1}}{h_j} &= (S_1)_{j-\frac{1}{2}},\\
\frac{\theta_j - \theta_{j-1}}{h_j} &= (Y_1)_{j-\frac{1}{2}},\\
\frac{\phi_j - \phi_{j-1}}{h_j} &= (Z_1)_{j-\frac{1}{2}},
\end{aligned} \tag{32}$$

Now the relation between the thickness

$$\begin{aligned}
&\frac{(V_1)_j - (V_1)_{j-1}}{h_j} - (U_1)^2{}_{j-\frac{1}{2}} + F_{j-\frac{1}{2}}(V_1)_{j-\frac{1}{2}} + 1\\
&- \alpha_1\left(F_{j-\frac{1}{2}}\left(\frac{(W_1)_j - (W_1)_{j-1}}{h_j}\right) - 2(U_1)_{j-\frac{1}{2}}(W_1)_{j-\frac{1}{2}}\right.\\
&\left.+ (V_1)^2{}_{j-\frac{1}{2}}\right) = 0,
\end{aligned} \tag{33}$$

$$\begin{aligned}
&\frac{(P_1)_j - (P_1)_{j-1}}{h_j} - (U_1)_{j-\frac{1}{2}}(P_1)_{j-\frac{1}{2}} + (F)_{j-\frac{1}{2}}(Q_1)_{j-\frac{1}{2}} + \gamma(\beta - \varepsilon)\\
&- \alpha_1\left(F_{j-\frac{1}{2}}\left(\frac{(S_1)_j - (S_1)_{j-1}}{h_j}\right) + (Q_1)_{j-\frac{1}{2}}(V_1)_{j-\frac{1}{2}} - (U_1)_{j-\frac{1}{2}}(S_1)_{j-\frac{1}{2}}\right.\\
&\left.- (P_1)_{j-\frac{1}{2}}(W_1)_{j-\frac{1}{2}}\right) = 0,
\end{aligned} \tag{34}$$

$$\begin{aligned}
&\left(1 + \frac{4}{3}R_d\right)\left(\frac{(Y_1)_j - (Y_1)_{j-1}}{h_j}\right) + \mathrm{Pr}F_{j-\frac{1}{2}}(Y_1)_{j-\frac{1}{2}}\\
&+ \mathrm{PrNb}(Y_1)_{j-\frac{1}{2}}(Z_1)_{j-\frac{1}{2}} + \mathrm{PrNt}(Y_1)_{j-\frac{1}{2}}{}^2 = 0,
\end{aligned} \tag{35}$$

$$\begin{aligned}
&\left(\frac{(Z_1)_j - (Z_1)_{j-1}}{h_j}\right) + \mathrm{Le}F_{j-\frac{1}{2}}(Z_1)_{j-\frac{1}{2}} + \frac{\mathrm{Nt}}{\mathrm{Nb}}\left(\frac{(Y_1)_j - (Y_1)_{j-1}}{h_j}\right)\\
&- \mathrm{Le}\beta_c\phi_{j-\frac{1}{2}} = 0.
\end{aligned} \tag{36}$$

Step 3: As Eqs. (34)–(36) are nonlinear, Newton linearization scheme is followed for converting the problem to linearized form.

$$\begin{aligned}
\delta F_j - \delta F_{j-1} - \frac{h_j}{2}((\delta U_1)_j + (\delta U_1)_{j-1}) &= (r_1)_{j-\frac{1}{2}},\\
(\delta U_1)_j - (\delta U_1)_{j-1} - \frac{h_j}{2}((\delta V_1)_j + (\delta V_1)_{j-1}) &= (r_2)_{j-\frac{1}{2}},\\
(\delta V_1)_j - (\delta V_1)_{j-1} - \frac{h_j}{2}((\delta W_1)_j + (\delta W_1)_{j-1}) &= (r_9)_{j-\frac{1}{2}},\\
\delta G_j - \delta G_{j-1} - \frac{h_j}{2}((\delta P_1)_j + (\delta P_1)_{j-1}) &= (r_3)_{j-\frac{1}{2}},\\
(\delta P_1)_j - (\delta P_1)_{j-1} - \frac{h_j}{2}((\delta Q_1)_j + (\delta Q_1)_{j-1}) &= (r_4)_{j-\frac{1}{2}},\\
(\delta Q_1)_j - (\delta Q_1)_{j-1} - \frac{h_j}{2}((\delta S_1)_j + (\delta S_1)_{j-1}) &= (r_{10})_{j-\frac{1}{2}},\\
\delta\theta_j - \delta\theta_{j-1} - \frac{h_j}{2}((\delta Y_1)_j + (\delta Y_1)_{j-1}) &= (r_{11})_{j-\frac{1}{2}},\\
\delta\phi_j - \delta\phi_{j-1} - \frac{h_j}{2}((\delta Z_1)_j + (\delta Z_1)_{j-1}) &= (r_{12})_{j-\frac{1}{2}},
\end{aligned} \tag{37}$$

$$\begin{aligned}
&\xi_1\delta F_j + \xi_2\delta F_{j-1} + \xi_3(\delta U_1)_j + \xi_4(\delta U_1)_{j-1} + \xi_5(\delta V_1)_j\\
&+ \xi_6(\delta V_1)_{j-1} + \xi_7(\delta W_1)_j + \xi_8(\delta W_1)_{j-1} = (r_5)_{j-\frac{1}{2}},
\end{aligned} \tag{38}$$

$$\begin{aligned}
&\psi_1\delta F_j + \psi_2\delta F_{j-1} + \psi_3(\delta U_1)_j + \psi_4(\delta U_1)_{j-1} + \psi_5(\delta W_1)_j\\
&+ \psi_6(\delta W_1)_{j-1} + \psi_7\delta G_j + \psi_8\delta G_{j-1}\\
&\psi_9\delta(P_1)_j + \psi_{10}(\delta P_1)_{j-1} + \psi_{11}\delta(Q_1)_j + \psi_{12}(\delta Q_1)_{j-1}\\
&+ \psi_{13}\delta(Q_1)_j + \psi_{14}(\delta Q_1)_{j-1} = (r_6)_{j-\frac{1}{2}},
\end{aligned} \tag{39}$$

$$\begin{aligned}
&\lambda_1\delta F_j + \lambda_2\delta F_{j-1} + \lambda_3(\delta Y_1)_j + \lambda_4(\delta Y_1)_{j-1} + \lambda_5(\delta Z_1)_j\\
&+ \lambda_6(\delta Z_1)_{j-1} = (r_7)_{j-\frac{1}{2}},
\end{aligned} \tag{40}$$

$$\begin{aligned}
&\gamma_1\delta F_j + \gamma_2\delta F_{j-1} + \gamma_3(\delta Y_1)_j + \gamma_4(\delta Y_1)_{j-1}\\
&\gamma_5\delta\phi_j + \gamma_6\delta\phi_{j-1} + \gamma_7(\delta Z_1)_j + \gamma_8(\delta Z_1)_{j-1} = (r_8)_{j-\frac{1}{2}}.
\end{aligned} \tag{41}$$

The associated boundary conditions take the form

$$\begin{aligned}
&\delta(V_1)_0 + 3\alpha_1((U_1)_0\delta(V_1)_0 + (V_1)_0\delta(U_1)_0) - \lambda\delta(U_1)_0\\
&= \lambda(U_1)_0 - (V_1)_0 - 3\alpha_1(U_1)_0(V_1)_0\\
&\qquad \lambda(P_1)_0(U_1)_0 - (Q_1)_0\\
&\delta(Q_1)_0 + \alpha_1\begin{pmatrix}(Q_1)_0\delta(P_1)_0 + (P_1)_0\delta(Q_1)_0\\ 2(Q_1)_0\delta(U_1)_0 + 2(U_1)_0\delta(Q_1)_0\end{pmatrix}\\
&\quad - \begin{pmatrix}\lambda(P_1)_0\delta(U_1)_0\\ -\lambda(U_1)_0\delta(P_1)_0\end{pmatrix} = -\alpha\begin{pmatrix}(Q_1)_0(P_1)_0\\ +2(U_1)_0(Q_1)_0\end{pmatrix}\\
&\delta F_0 = 0 = \delta G_0 = \delta\theta_0 = \delta\phi_0, \delta(U_1)_J = 0 = \delta(P_1)_J = \delta\theta_J\\
&= \delta\phi_J
\end{aligned} \tag{42}$$

where

$$(r_1)_{j-\frac{1}{2}} = F_{j-1} - \delta F_j + \frac{h_j}{2}((U_1)_j + (U_1)_{j-1}),$$

$$(r_2)_{j-\frac{1}{2}} = (U_1)_{j-1} - (\delta U_1)_j + \frac{h_j}{2}((V_1)_j + (V_1)_{j-1}),$$

$$(r_3)_{j-\frac{1}{2}} = G_{j-1} - \delta G_j + \frac{h_j}{2}((P_1)_j + (P_1)_{j-1}),$$

$$(r_4)_{j-\frac{1}{2}} = (P_1)_{j-1} - (P_1)_j + \frac{h_j}{2}((Q_1)_j + (Q_1)_{j-1}),$$

$$(r_9)_{j-\frac{1}{2}} = (V_1)_{j-1} - (\delta V_1)_j + \frac{h_j}{2}((W_1)_j + (W_1)_{j-1}),$$

$$(r_{10})_{j-\frac{1}{2}} = (Q_1)_{j-1} - (Q_1)_j + \frac{h_j}{2}((S_1)_j + (S_1)_{j-1}),$$

$$(r_{11})_{j-\frac{1}{2}} = \theta_{j-1} - \theta_j + \frac{h_j}{2}((Y_1)_j + (Y_1)_{j-1}),$$

$$(r_{12})_{j-\frac{1}{2}} = \phi_{j-1} - \phi_j + \frac{h_j}{2}((Z_1)_j + (Z_1)_{j-1}),$$

$$(r_5)_{j-\frac{1}{2}} = (V_1)_{j-1} - (V_1)_j + h_j(U_1)^2{}_{j-\frac{1}{2}} - h_j F_{j-\frac{1}{2}}(V_1)_{j-\frac{1}{2}} - h_j + \alpha_1 h_j\left(F_{j-\frac{1}{2}}\left(\frac{(W_1)_j - (W_1)_{j-1}}{h_j}\right) - 2h_j(U_1)_{j-\frac{1}{2}}(W_1)_{j-\frac{1}{2}} + h_j(V_1)^2{}_{j-\frac{1}{2}}\right),$$

$$(r_6)_{j-\frac{1}{2}} = (P_1)_{j-1} - (P_1)_j + h_j(U_1)_{j-\frac{1}{2}}(P_1)_{j-\frac{1}{2}} - h_j(F)_{j-\frac{1}{2}}(Q_1)_{j-\frac{1}{2}} - h_j\gamma(\beta - \varepsilon) + h_j\alpha_1\left(F_{j-\frac{1}{2}}\left(\frac{(S_1)_j - (S_1)_{j-1}}{h_j}\right) + (Q_1)_{j-\frac{1}{2}}(V_1)_{j-\frac{1}{2}} - (U_1)_{j-\frac{1}{2}}(S_1)_{j-\frac{1}{2}} - (P_1)_{j-\frac{1}{2}}(W_1)_{j-\frac{1}{2}}\right),$$

$$(r_7)_{j-\frac{1}{2}} = \left(1 + \frac{4}{3}R_d\right)((Y_1)_{j-1} - (Y_1)_j) - h_j \mathrm{Pr} F_{j-\frac{1}{2}}(Y_1)_{j-\frac{1}{2}} - h_j \mathrm{PrNb}(Y_1)_{j-\frac{1}{2}}(Z_1)_{j-\frac{1}{2}} - h_j \mathrm{PrNt}(Y_1)_{j-\frac{1}{2}}{}^2,$$

$$(r_8)_{j-\frac{1}{2}} = ((Z_1)_{j-1} - (Z_1)_j) - h_j \mathrm{Le} F_{j-\frac{1}{2}}(Z_1)_{j-\frac{1}{2}} - h_j\frac{\mathrm{Nt}}{\mathrm{Nb}}\left(\frac{(Y_1)_j - (Y_1)_{j-1}}{h_j}\right) + h_j \mathrm{Le}\beta_c\phi_{j-\frac{1}{2}}.$$

Step 4: After writing Eqs. (37)–(41) in tri-diagonal matrix form in which each element is a matrix of order 12 × 12, the following program have been followed to compute tri-diagonal matrix for the fixed values of involved parameters.

```
TriMat[ma_, md_, mc_, mb_, n_] := Module[{AA = ma, BB = mb, c = mc, d = md, k, δ},
δ = Table[{{0}, {0}, {0}, {0}, {0}, {0}, {0}, {0}, {0}, {0}, {0}, {0}}, {n + 1}];
For[k = 2, k ≤ n + 1, k + +,
d[[k]] = d[[k]] − AA[[k − 1]]. Inverse[d[[k − 1]]]. c[[k − 1]];
BB[[k]] = BB[[k]] − AA[[k − 1]]. Inverse[d[[k − 1]]]. BB[[k − 1]];];
δ[[n + 1]] = Inverse[d[[n + 1]]]. BB[[n + 1]];
For[k = n, 1 ≤ k, k − −,
δ[[k]] = Inverse[d[[k]]]. BB[[k]] − Inverse[d[[k]]]. c[[k]]. δ[[k + 1]]];
Return[δ];]
```

4 Validation of results

The results are validated in Table 1 using the analysis of Li *et al.* [47] for limiting case. Clearly a fine accuracy is noted between both investigations (Table 1).

5 Results and discussion

To discuss the influence of emerging parameters on flow phenomenon, the graphical analysis has been performed. In order to observe the shear-thinning effects associated with the viscoelastic fluid, the value of n is chosen to be 0.5. Figure 2 is plotted to discuss the impact of slip parameter on both axial velocity $F'(\eta)$ and tangential velocity $G'(\eta)$ when $\alpha_1 = 0.0$ for viscous flow case and $\alpha_1 = 1.0$ for viscoelastic flow case. The decrement for axial component is preserved by increasing the slip parameter λ. As λ has inverse relation with slip, when λ increases, slip decreases which also restricts the movement of fluid in the axial direction and as a result, the velocity of the fluid reduces. Furthermore, the decline in velocity is large for viscoelastic fluid as compared to viscous fluid over lubricated surface. The decline in velocity due to viscoelasticity of the fluid is obvious. Because, as the viscoelastic parameter is increased,

Table 1: Numerical computations for $h'(0)$ when $\alpha_1 = 0.647903$ and $\lambda \to \infty$ using the analysis of Li *et al.* [47]

ε	Li *et al.* [47]	Present results
0.0	1.406370	1.406375
5.0	−4.756560	−4.756575
−5.0	7.569310	7.569312

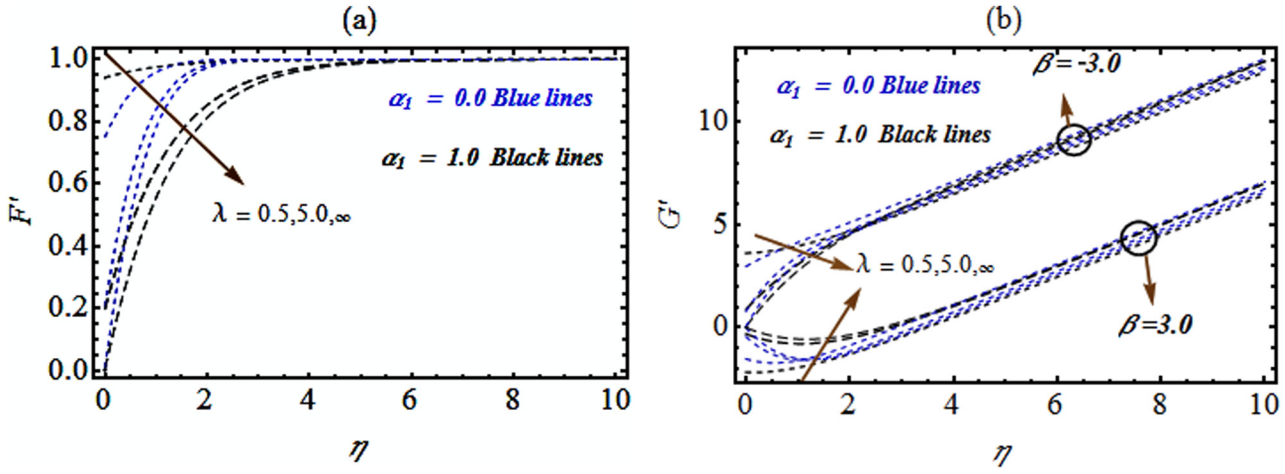

Figure 2: Impact of λ on (a) axial velocity F' and (b) transverse velocity G'.

the rheology of the fluid restricts the transport of the fluid near the surface and it causes the decline in the axial velocity of the fluid. Due to baring the creeping flow and stress relaxation properties of viscoelastic fluid, this theoretical model has many applications in the polymer industry. Due to these rheological properties, it is usual to predict the product quality and time- and cost-related developments of process at industrial level. The tangential velocity of both viscous and viscoelastic fluid is a decreasing function of the slip parameter over a lubricated surface. A similar trend is followed by both $\beta = -3.0$ and $\beta = 3.0$ but the decline is large for viscoelastic fluid as compared to viscous fluid. This shows that lubrication reduces the friction between the flat surface and the moving layers of the fluid. Therefore, lubrication has many applications in machinery components and it reduces the friction between the machinery components and fluid layers and rises the polymer process. Figure 3 concludes the association of slip factor λ with temperature field and profile of concentration for both viscous and viscoelastic fluids. Both temperature and concentration profiles are increasing function of slip parameter λ. It is noted that over flat surface, the temperature of nanofluid is large. The reason for this fact is that due to restriction of flow, the internal kinetic energy rises between the layers for nanomaterials which convey the enhanced thermal phenomenon. Due to the presence of lubrication film, formed between the surfaces, polymer process is done smoothly by reducing friction, which improves the performance and efficiency. Furthermore, the increase is large for viscoelastic model compared to that of the viscous fluid. This response is already reported in literature. The thermophoresis impact for temperature and concentration framework is visualized *via* Figure 4 over a lubricated surface. It is noted that both temperature profile and nanoparticles concentration profile increase with the

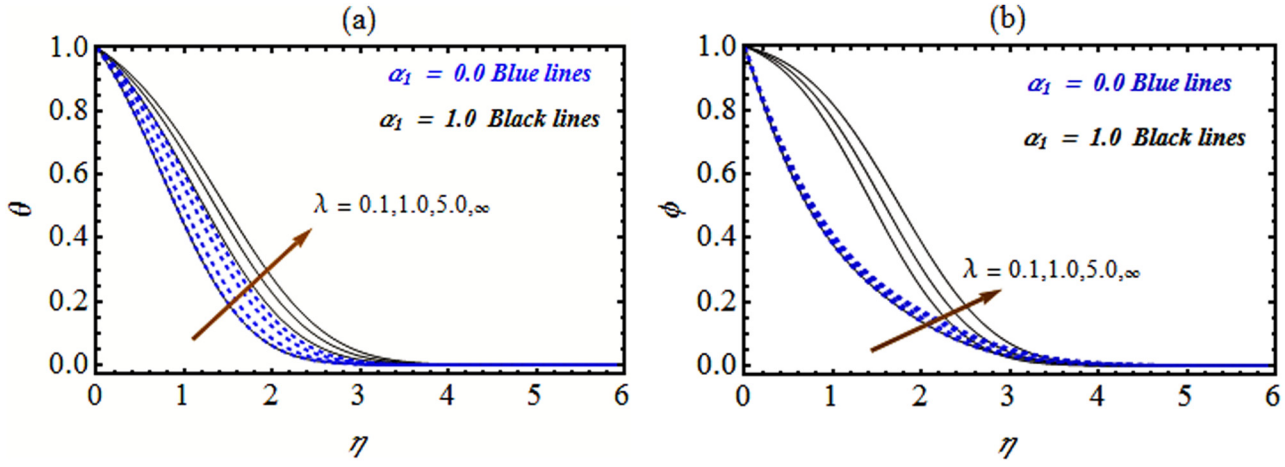

Figure 3: Impact of λ on (a) temperature θ and (b) concentration ϕ.

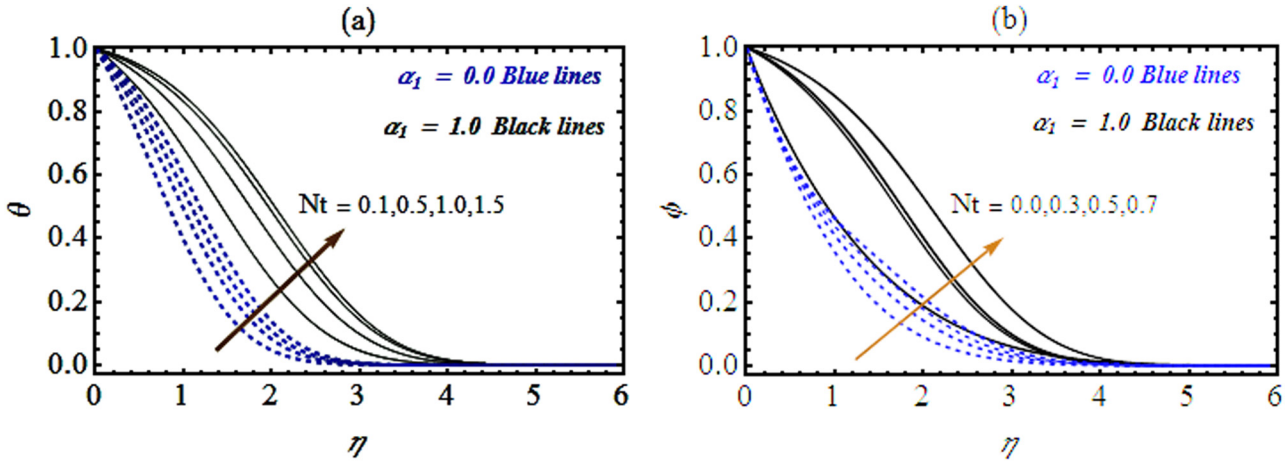

Figure 4: Impact of Nt on (a) temperature θ and (b) concentration ϕ.

increase in the thermophoresis diffusion of nanoparticles in nanofluid. Furthermore, the increasing trend is followed by thermophoresis parameter at large scale for viscoelastic fluid as compared to viscous fluid. As thermophoresis force is recognized as transport force which arises due to the temperature gradient, the temperature gradient causes the migration of nanoparticles from hot zone to cold zone which rises the heat transfer. Also, the viscoelasticity of the fluid reduces the boundary layer movement in the fluid which is responsible for the large rise of temperature against thermophoresis. The justification of Brownian constant for temperature profile of nanoparticles and nanoparticle concentration profile is reported in Figure 5 for several values of α_1. The temperature of both viscous and viscoelastic fluid is an increasing function of Brownian motion parameter Nb over a lubricated surface. The nanofluid concentration show decrement with upraise function of Brownian motion over a lubricated surface for both $\alpha_1 = 0.0$ and $\alpha_1 = 2.0$. Figure 6(a) shows the effect of Rd on $\theta(\eta)$ over a lubricated surface for both viscous as well as viscoelastic fluid. The increasing behavior is noticed for temperature as the value of radiation is increased. The deduced enhancement in temperature is due to the fact that radiation parameter causes the rise in temperature over the surface which strongly transfers the heat into the transporting fluid. By increasing the thermal radiation parameter, more heat is added to the system and as a result, the temperature of both viscous and viscoelastic fluids increases. In Figure 6(b), the qualitative impact of chemical reaction parameter on the concentration of nanofluid is reported for several values of α. The enhancement in reactive constant reduces effectively the concentration impact for both viscous and viscoelastic nanofluids. However, the impact of chemical reaction parameter can control the decrease noticed for viscous case instead of viscoelastic fluids over a

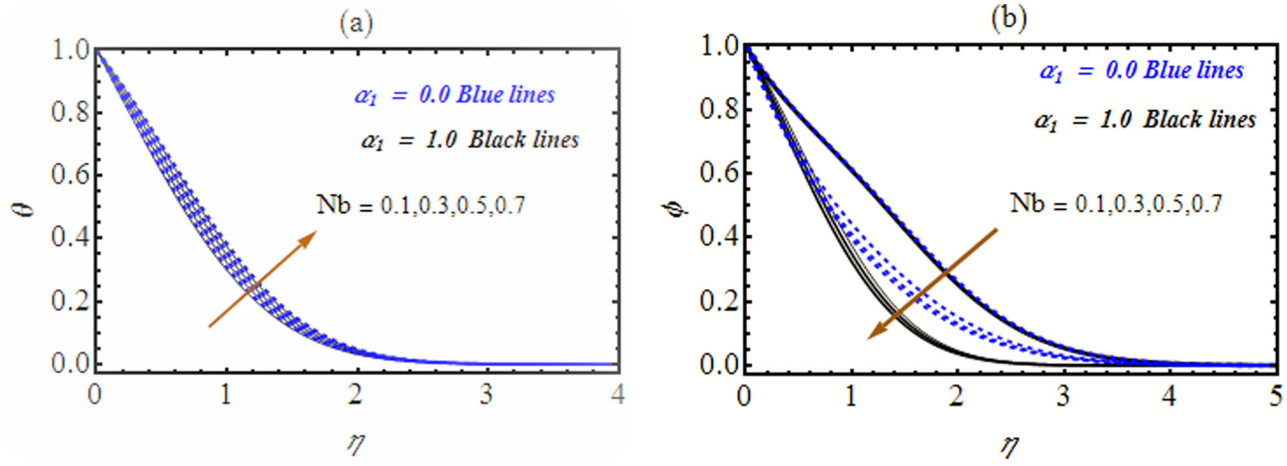

Figure 5: Impact of Nb on (a) temperature θ and (b) concentration ϕ.

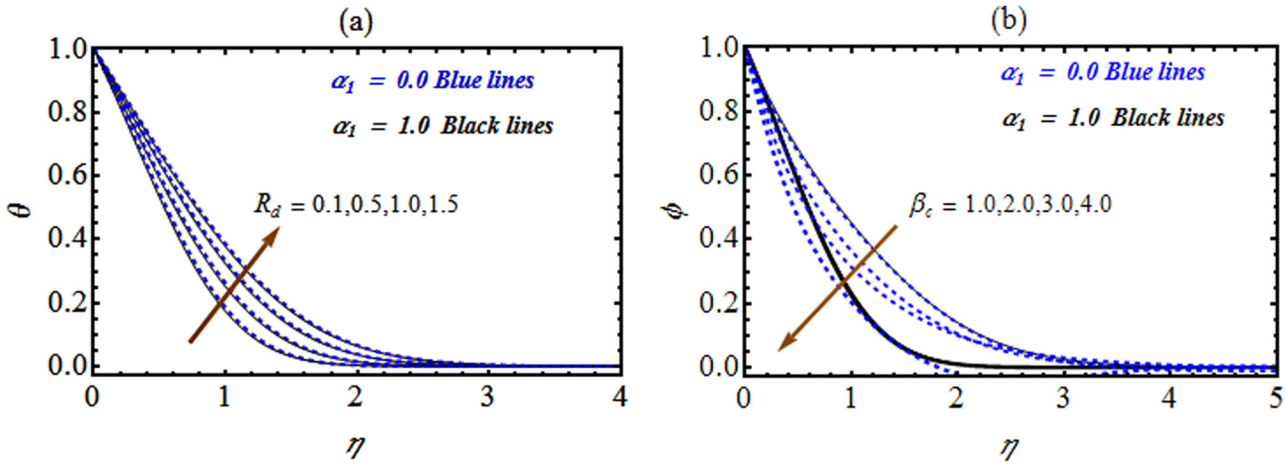

Figure 6: Impact of (a) Rd on temperature θ and (b) βc concentration ϕ.

lubricated surface. The concentration profile decline suggests that in various industrial processes, the optimization of nanoparticle concentration and the role of chemical reactions are significant factors.

The impact of slip parameter λ on the skin friction coefficient for various values of viscoelastic parameter α_1 is reported and displayed in Table 2. It is noted that the rising values of slip parameter enhance the numerical values of skin friction coefficient for several values of viscoelastic parameter α_1. Lower magnitude in wall shear force is preserved under slip constraints ($\lambda \to 0$). The viscoelastic factor tends to improve the wall shear force when specific role of slip is observed. However, no-slip constraint assumptions lead to decrement in shear force with the increase in viscoelastic parameter. In Table 3, the response of Nusselt number against thermophoresis parameter Nt, Brownian motion parameter Nb and thermal radiation parameter R_d for several values of viscoelastic parameter are displayed. The declining impact on Nusselt number for Nt and Nb against several values of α_1 has been noticed. Furthermore, Nusselt number is an increasing function of viscoelastic parameter α_1. On the other hand, radiation parameter rises the Nusselt number for both viscous fluid as well as viscoelastic fluid. The significance of Nt, Nb and β_c for both viscous and viscoelastic fluid parameters on Sherwood number is presented in Table 4. It is noted that thermophoresis parameter Nt declines the Sherwood

Table 2: Variation in skin friction coefficient against λ and α_1 with x_1 = 1.0

λ	α_1 = 0.0	α_1 = 0.1	α_1 = 1.0
0.1	0.1704616695	0.1771405914	0.2240388946
0.5	0.7003608605	0.7387329469	0.9936887763
1.0	1.1336966286	1.1990725778	1.6938969768
5.0	2.1352423991	2.1486662335	2.47150481294
∞	2.6391568934	2.5008565373	1.96502524986

Table 3: Variation in Nusselt number $\frac{Nu_x}{\sqrt{Re_x}}$ against Nt, Nb and R_d with λ = 0.1

Nt	Nb	R_d	$\frac{Nu_x}{\sqrt{Re_x}}$		
			α_1 = 0.0	α_1 = 0.1	α_1 = 1.0
0.1	0.5	0.5	0.96959225	0.97106766	0.97692570
0.5			0.78070647	0.78198540	0.78706524
1.0			0.59597658	0.59703442	0.60125121
	0.1		0.81200024	0.81335667	0.81873316
	0.2		0.75337949	0.75465794	0.75973840
	0.3		0.69788065	0.69908413	0.70387232
		0.0	0.468169520	0.46938998	0.47416639
		1.0	0.88499335	0.88618196	0.89112179
		2.0	1.19221428	1.19335358	1.19843002

Table 4: Variation in Sherwood number $\frac{Sh}{\sqrt{Re_x}}$ against Nt, Nb and β_c with λ = 0.1

Nt	Nb	β_c	$\frac{Sh}{\sqrt{Re_x}}$		
			α_1 = 0.0	α_1 = 0.1	α_1 = 1.0
0.1	0.5	0.5	0.676456252	0.67658664	0.67733232
0.5			0.56198246	0.56142305	0.55964073
1.0			0.60628131	0.60515755	0.60133143
	0.1		−1.22761585	−1.23672748	−1.27025831
	0.2		−0.06427519	−0.06840306	−0.08332812
	0.3		0.31547904	0.31302484	0.30428581
		0.0	−0.15126240	−0.15590275	−0.17313797
		1.0	0.62113443	0.61956892	0.61376748
		2.0	1.02213652	1.02139495	1.01852021

number, while on the other hand both Brownian motion parameter Nb and chemical reaction parameter β_c rises the Sherwood number. The viscoelastic parameter reduces the Sherwood number.

6 Concluding remarks

The numerical framework for radiative viscoelastic nanofluid problem with lubricated surface has been endorsed. The role of chemical species with first order are entertained. The Keller Box technique is utilized for formulated problem. The assessment of flow behavior is observed for viscous fluid case and under no-slip assumptions. Major outcomes are as follows:

1) A reduction in the axial and tangential velocities have been observed when the role of lubrication phenomenon due to flat surface is studied.

2) For slip constraints, the decrement in velocity is observed subject to the slip effects. Such features are more dominant for viscoelastic fluid.

3) The temperature profile increases with the increase in the thermophoresis diffusion, slip parameter and Brownian motion parameter.

4) Concentration profile is a decreasing function of Brownian motion and an increasing function of thermophoresis diffusion parameter.

5) Thermal radiation parameter enhances the temperature of nanofluid over a lubricated surface.

6) The skin friction is an increasing function of viscoelastic parameter for full slip and decreases for no-slip case.

7) Both Brownian motion parameter and thermophoresis parameter reduces while radiation parameter rises the Nusselt number.

8) The Nusselt number increases with the increase in viscoelastic parameter, while Sherwood number reduces by enhancing the viscoelastic parameter.

9) Brownian motion parameter and chemical reaction parameter increases the Sherwood number.

Acknowledgments: Researchers Supporting Project number (RSPD2023R1060), King Saud University, Riyadh, Saudi Arabia.

Funding information: This project is funded by King Saud University, Riyadh, Saudi Arabia.

Author contributions: All authors have accepted responsibility for the entire content of this manuscript and approved its submission.

Conflict of interest: The authors state no conflict of interest.

Data availability statement: The datasets generated and/or analysed during the current study are available from the corresponding author on reasonable request.

References

[1] Hiemenz K. Die Grenzschicht an einem in den gleichformigen Flussigkeitsstrom eingetauchten geraden Kreiszylinder. Dinglers Polytech J. 1911;326:321–4.
[2] Homann F. Der Einfluss grosser Zähigkeit bei der Strömung um den Zylinder und um die Kugel. ZAMM-J Appl Math Mech/Z Angew Math Mech. 1936;16(3):153–64.
[3] Hannah DM. Forced flow against a rotating disc. London: Aeronautical Research Council; 1947.
[4] Rott N. Unsteady viscous flow in the vicinity of a stagnation point. Quart Appl Math. 1956;13(4):444–51.
[5] Weidman PD, Mahalingam S. Axisymmetric stagnation-point flow impinging on a transversely oscillating plate with suction. J Eng Math. 1997;31(2):305–18.
[6] Mahapatra TR, Gupta AS. Stagnation-point flow towards a stretching surface. Can J Chem Eng. 2003;81(2):258–63.
[7] Lok YY, Amin N, Pop I. Non-orthogonal stagnation point flow towards a stretching sheet. Int J Non-Linear Mech. 2006;41(4):622–7.
[8] Nadeem S, Hussain A, Majid K. Stagnation flow of a Jeffrey fluid over a shrinking sheet. Z Naturforsch A. 2010;65(6–7):540–8.
[9] Weidman PD, Sprague MA. Flows induced by a plate moving normal to stagnation-point flow. Acta Mech. 2011;219(3):219–29.
[10] Weidman PD. Obliquely intersecting Hiemenz flows: a new interpretation of Howarth stagnation-point flows. Fluid Dynam Res. 2012;44(6):065509.
[11] Stuart JT. The viscous flow near a stagnation point when the external flow has uniform vorticity. J Aerosp Sci. 1959;26(2):124–5.
[12] Tamada K. Two-dimensional stagnation-point flow impinging obliquely on a plane wall. J Phys Soc Japan. 1979;46(1):310–1.
[13] Dorrepaal JM. An exact solution of the Navier-Stokes equation which describes non-orthogonal stagnation-point flow in two dimensions. J Fluid Mech. 1986;163:141–7.
[14] Reza M, Gupta AS. Steady two-dimensional oblique stagnation-point flow towards a stretching surface. Fluid Dynam Res. 2005;37(5):334.
[15] Weidman PD, Putkaradze V. Axisymmetric stagnation flow obliquely impinging on a circular cylinder. Eur J Mech-B/Fluids. 2003;22(2):123–31.
[16] Lok YY, Pop I, Chamkha AJ. Non-orthogonal stagnation-point flow of a micropolar fluid. Int J Eng Sci. 2007;45(1):173–84.
[17] Dandapat BS, Gupta AS. Flow and heat transfer in a viscoelastic fluid over a stretching sheet. Int J Non-Linear Mech. 1986;24(3):215–9.
[18] Mahapatra T, Gupta AS. Heat transfer in stagnation-point flow towards a stretching sheet. Heat Mass Transf. 2002;38(6):517–21.
[19] Hayat T, Sajid M. Analytic solution for axisymmetric flow and heat transfer of a second-grade fluid past a stretching sheet. Int J Heat Mass Transf. 2007;50(1–2):75–84.

[20] Attia HA. Hiemenz flow through a porous medium of a non-Newtonian Rivlin-Ericksen fluid with heat transfer. J Appl Sci Eng. 2009;12(3):359–64.
[21] Bachok N, Ishak A, Nazar R, Pop I. Flow and heat transfer at a general three-dimensional stagnation point in a nanofluid. Phys B: Cond Matt. 2010;405(24):4914–8.
[22] Arshad A, Sajid M, Rana MA, Mahmood K. Numerical simulation of heat transfer features in oblique stagnation-point flow of Jeffrey fluid. AIP Adv. 2018;8(10):105111.
[23] Bano A, Sajid M, Mahmood K, Rana MA. An oblique stagnation point flow towards a stretching cylinder with heat transfer. Phys Scr. 2019;95(1):015704.
[24] Labropulu F, Li D, Pop I. Non-orthogonal stagnation-point flow towards a stretching surface in a non-Newtonian fluid with heat transfer. Int J Therm Sci. 2010;49(6):1042–50.
[25] Abbasi A, Farooq W, Ghachem K, Shabir S, Elmonser H, Khan SU, et al. Nonlinear radiative oblique stagnation point flow of viscoelastic fluid due to stretching cylinder with polymer processing applications. Waves Random Complex Media. 2022;33(3):825–40.
[26] Choi SU, Eastman JA. Enhancing thermal conductivity of fluids with nanoparticles (No. ANL/MSD/CP-84938; CONF-951135-29). Argonne, IL (United States): Argonne National Lab. (ANL); 1995.
[27] Das M, Patil S, Bhargava N, Kang JF, Riedel LM, Seal S, et al. Autocatalytic ceria nanoparticles offer neuroprotection to adult rat spinal cord neurons. Biomaterials. 2007;28(10):1918–25.
[28] Buongiorno J. Convective transport in nanofluids. J Heat Transf. 2006;128(3):240–50.
[29] Hamid RA, Nazar R, Pop I. Non-alignment stagnation-point flow of a nanofluid past a permeable stretching/shrinking sheet: Buongiorno's model. Sci Rep. 2015;5(1):1–11.
[30] Roşca AV, Roşca NC, Pop I. Stagnation point flow of a nanofluid past a non-aligned stretching/shrinking sheet with a second-order slip velocity. Int J Numer Methods Heat Fluid Flow. 2018;29(2):738–62.
[31] Abbasi A, Farooq W, Mabood F, Hussain Z. Finite difference simulation for oblique stagnation point flow of viscous nanofluid towards a stretching cylinder. Phys Scr. 2020;96(1):015212.
[32] Abbasi A, Mabood F, Farooq W, Hussain Z. Non-orthogonal stagnation point flow of Maxwell nano-material over a stretching cylinder. Int Commun Heat Mass Transf. 2021;120:105043.
[33] Mahmood K, Sajid M, Ali N, Arshad A, Rana MA. Effects of lubrication in the oblique stagnation-point flow of a nanofluid. Microfluid Nanofluid. 2017;21(5):1–11.
[34] Abbasi A, Farooq W, Riaz I. Stagnation point flow of Maxwell nanofluid containing gyrotactic micro-organism impinging obliquely on a convective surface. Heat Transf. 2020;49(5):2977–99.
[35] Nadeem S, Khan AU. MHD oblique stagnation point flow of nanofluid over an oscillatory stretching/shrinking sheet: existence of dual solutions. Phys Scr. 2019;94(7):075204.
[36] Bao Y, Huang A, Zheng X, Qin G. Enhanced photothermal conversion performance of MWCNT/SiC hybrid aqueous nanofluids in direct absorption solar collectors. J Mol Liq. 2023;387:122577.
[37] Selim MM, El-Safty S, Tounsi A, Shenashen M. Review of the impact of the external magnetic field on the characteristics of magnetic nanofluids. Alex Eng J. 2023;76:75–89.
[38] Hanafi NSM, Ghopa WAW, Zulkifli R, Sabri MAM, Zamri WFHW, Ahmad MIM. Mathematical formulation of Al_2O_3-Cu/water hybrid nanofluid performance in jet impingement cooling. Energy Rep. 2023;9:435–46.
[39] Ghafouri A, Toghraie D. Novel multivariate correlation for thermal conductivity of SiC-MgO/ethylene glycol nanofluid based on an experimental study. Mater Sci Eng B. 2023;297:116771.
[40] Sundar LS. Synthesis and characterization of hybrid nanofluids and their usage in different heat exchangers for an improved heat transfer rates: A critical review. Eng Sci Technol Int J. 2023;44:101468.
[41] Zhao C, Cheung CF, Xu P. High-efficiency sub-microscale uncertainty measurement method using pattern recognition. ISA Trans. 2020;101:503–14.
[42] Gao Z, Hong S, Dang C. An experimental investigation of subcooled pool boiling on downward-facing surfaces with microchannels. Appl Therm Eng. 2023;226:120283.
[43] Tian Z, Zhang Y, Zheng Z, Zhang M, Zhang T, Jin J, Zhang Q. Gut microbiome dysbiosis contributes to abdominal aortic aneurysm by promoting neutrophil extracellular trap formation. Cell Host Microbe. 2022;30(10):1450–63.
[44] Dai Z, Xie J, Jiang M. A coupled peridynamics–smoothed particle hydrodynamics model for fracture analysis of fluid–structure interactions. Ocean Eng. 2023;279:114582.
[45] Bian Y, Zhu S, Li X, Tao Y, Nian C, Zhang C, et al. Bioinspired magnetism-responsive hybrid microstructures with dynamic switching toward liquid droplet rolling states. Nanoscale. 2023;15(28):11945–54.
[46] Bai B, Rao D, Chang T, Guo Z. A nonlinear attachment-detachment model with adsorption hysteresis for suspension-colloidal transport in porous media. J Hydrol. 2019;578:124080.
[47] Li D, Labropulu F, Pop I. Oblique stagnation-point flow of a viscoelastic fluid with heat transfer. Int J Non-Linear Mech. 2009;44:1024–30.